Chiral Films

International Edition: DOI: 10.1002/anie.201509068
German Edition: DOI: 10.1002/ange.201509068

Oriented Chiral DNA–Silica Film Guided by a Natural Mica Substrate

Yuanyuan Cao, Kunche Kao, Chungyuan Mou, Lu Han, and Shunai Che**

Abstract: *The formation of highly ordered chiral organic/inorganic films with high density and long-range orientation is important in constructing chiral devices, such as broadband polarization devices, liquid-crystal displays, or negative-reflection materials. A feasible strategy is presented to fabricate three-dimensional mesostructured chiral DNA–silica assemblies into large-scale oriented arrangements. The highly ordered film was aligned by a mica crystal substrate with the bridging effect of suitable divalent metal ions, followed by the growth of the DNA–silica composite by bottom-up assembly with a "quartet templating" method. This simple and effective route would perform well in the alignment and arrangement of highly charged biomolecules, such as polypeptides, proteins, viruses, and their inorganic assemblies, and furthermore could allow the fabrication of chiral optical materials with long-range ordering.*

The precise engineering of nanostructures over a macroscopic surface into highly ordered three-dimensional (3D) arrays is a substantial challenge in many applications in nanotechnology.[1] Among them, chiral nanostructures are of great interest.[2] The significant aspects of chiral devices, especially chiral films such as broadband polarizers,[3] chiral liquid crystals,[4] and chiral filters,[5] often arise from their long-range arrangement. The template-assisted self-assembly (TASA) method to guide suitable chiral molecules to assemble into 3D large arrays is an effective strategy to fabricate long-range ordered chiral films. The combination of top-down substrate design and bottom-up molecular self-assembly would enable us to integrate individual nanostructures into arranged functional devices.[6]

As one of the most attractive biomolecular building blocks, DNA molecules provide high stereoregularity for building artificial nanostructures and possess inherent chirality to assemble into delicate chiral materials.[1b,7] Using elaborate intermolecular interactions, DNA can position materials with precision into periodic or aperiodic structures.[8] Thus, controlling the orientation and arrangement of DNA assembles on supporting substrates through TASA may be the fine approach for the fabrication of highly ordered films with chiral structures.

Previously, we successfully oriented and selectively arranged achiral 2D mesostructured DNA–silica platelets on the surface of a lithographic silicon substrate through TASA.[9] Furthermore, chiral DNA–silica impellers have also been fabricated on silica wafers, showing both absorption- and scattering-based optical activity (OA).[10] Unfortunately, the randomly distributed impellers suffer from weak OA, raising the requirements in terms of controlling the orientation of chiral DNA–silica assemblies. Meanwhile, the lithographic process is energy-intensive, and the resolution is limited to 7 nm length scales.[11] It is necessary to choose a new substrate to align the structure.

Despite commonly used substrates having organized lithographic patterns, flat crystalline substrates (highly ordered large-scale organizations that arisen from natural confined growth) such as mica,[12] graphene,[13] and monocrystalline silicon wafers,[14] are regarded as good candidates to guide the ordered epitaxial growth of nanostructures. These readily available templates often provide guiding effects, which are attributed to their atomic-scale crystal structure. Herein, muscovite mica sheets, a low-cost natural laminar mineral that has atomically flat crystalline surfaces with a 2D hexagonal arrangement and sufficient charge,[15] are expected to behave both as the substrate and the template that will control the orientation of chiral DNA–silica films. The DNA–silica chiral mesostructure was assembled by the silicification of the chiral packing structure of short B-form DNA molecules (100–250 bp after sonication treatment; Supporting Information, Figure S1) in the presence of *N*-trimethoxysilylpropyl-*N*,*N*,*N*-trimethylammonium chloride (TMAPS) and a silica source, tetraethoxysilane (TEOS), via a co-structure direction method.[16] The cationic silane TMAPS was applied as the linkage between DNA molecules and silica source. The Mg^{2+} ion was introduced as both the chiral inducing agent and the bridging ion connecting the crystalline mica and DNA–silica assembly to control the direction of the chiral film.

Figure 1a shows scanning electron microscopy (SEM) images of the DNA–silica film synthesized without Mg^{2+} ions; the film is composed of randomly distributed vertical blades with thicknesses of 50–100 nm (inset of Figure $1a_2$), corresponding to the length of the DNA molecule employed. The heights of the blades are about 300 nm, judging from the side view of the image (Figure $1a_3$). In this case, the flat achiral 2D DNA–silica plates that form on the mica substrate do not exhibit chirality, as indicated by the powder remaining in solution (Supporting Information, Figure S2a,b). The film that formed is called an achiral DNA–silica film (ADSF).

With the addition of Mg^{2+} ions, the blades adopted an oriented, chiral feature, as shown in Figure 1b. This chiral

[*] Y. Cao, Dr. L. Han, Prof. Dr. S. Che
School of Chemistry and Chemical Engineering, State Key Laboratory of Metal Matrix Composites, Shanghai Jiao Tong University
800 Dongchuan Road, Shanghai, 200240 (P.R. China)
E-mail: luhan@sjtu.edu.cn
chesa@sjtu.edu.cn
Homepage: http://che.sjtu.edu.cn
Dr. K. Kao, Prof. Dr. C. Mou
Department of Chemistry, National Taiwan University
Taipei, 10617 (Taiwan)

Supporting information for this article is available on the WWW under http://dx.doi.org/10.1002/anie.201509068.

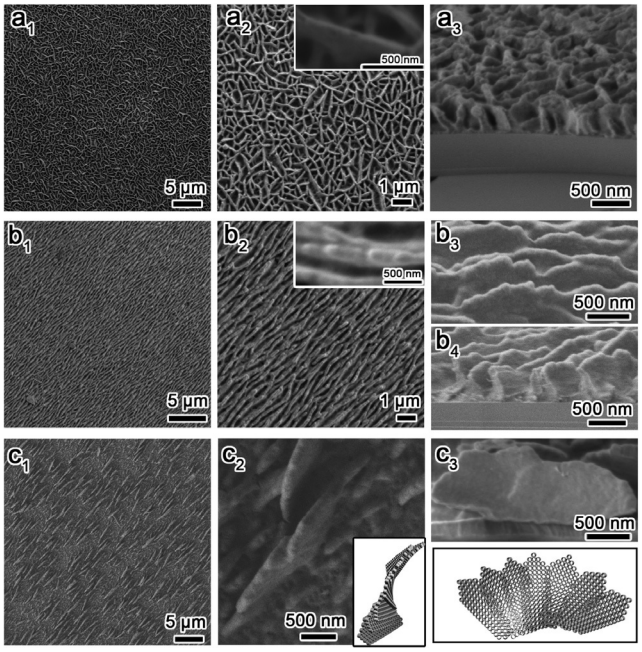

Figure 1. a) SEM images of the ADSF at low and high magnifications, top view (a_1 and a_2) and side view (a_3). b) SEM images of the OCDSF at low and high magnifications, top view (b_1 and b_2) and side view (b_3 and b_4). c) SEM images of the sparse OCDSF at low and high magnifications, top view (c_1 and c_2) and side view (c_3). The molar composition of the synthesis gel is DNA (phosphate groups)/Mg^{2+}/TMAPS/TEOS/H_2O = 1:0:6:15:17857 (a) and 1:1:6:15:17857 (b and c).

film, called an oriented chiral DNA–silica film (OCDSF), is composed of numerous blades with a uniform thickness of 100–150 nm, aligned tightly along one horizontal direction and over a continuous long range (tens of micrometers; Supporting Information, Figure $1b_1$ and $1b_2$). The top view image of the OCDSF shows that the edges of the blades contain many bulges and twist slightly (inset of Figure $1b_2$). The side view of the blades confirms the twisting and also shows an uneven wave-like morphology with 200–500 nm in height (Figure $1b_3$ and $1b_4$). The regular alignment is visible at the macroscopic scale of 1 cm^2, showing a uniform appearance under cross-polarized light (Supporting Information, Figure S3a) and naked-eye observation (Figure S3b). The chiral impeller morphology of the powder products remaining in the reaction solution (Supporting Information, Figure S4a) shows the right-handed stacking of the left-handed twisting petals. This distortion would force the edge of the particle to crack into an impeller-like conformation.[10,17] The high density of DNA molecules on the small substrate causes increasing steric hindrance, preventing the formation of totally impeller-like cracks but remaining only nuanced bulges. Moreover, the end-to-end connection of the vertically cambered blades, assisted by the templating effect of the mica surface, resulting in a long-range wave-like morphology.

To obtain detailed information of the blades, we prepared a sparse film by pre-treating the mica substrate with a lengthy aqueous immersion step. The extended immersion in water results in the abundant hydration of the mica surface, thus preventing the effective anchoring of DNA and producing sparsely distributed blades. As shown in Figure $1c_1$, the blades of the OCDSF are separated into short blades while keeping a uniform orientation. As shown in Figure $1c_2$ (top view) and $1c_3$ (side view), the individual blades are composed of stacked small petals with cracks on the edges and show cambered shapes with lengths of about 2.5 μm and a gentle right-handed distortion along the horizontal long axis, which is illustrated in the model. The right-handed stacking of the cracked blades reveals the helical morphology and induces the greater thickness of the blades than an individual achiral plate.

The long-range ordering of the OCDSF was further confirmed by a grazing-incidence small-angle X-ray scattering (GISAXS) measurement (Figure 2A; Supporting Information, Figure S5). The strongest reflection intensities appear

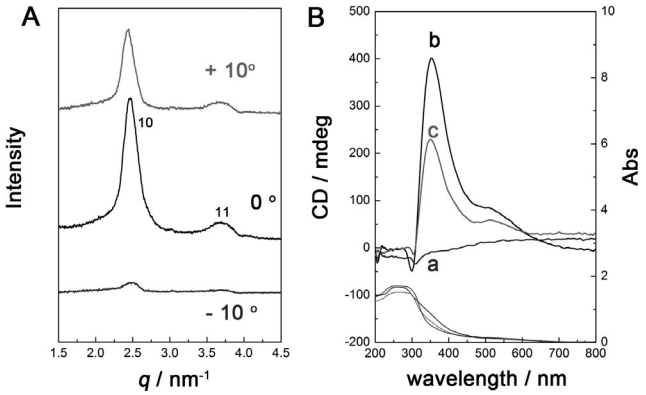

Figure 2. The long-range ordering of the OCDSF and the OA of the films shown in Figure 1. A) Fan-shape integration of the GISAXS patterns of the OCDSF with rotations of 0°, +10°, and −10°. B) DRCD and UV/Vis spectra of the films shown in Figure 1 measured with a white backboard.

when the blades are perpendicular to the X-ray beam. Rotating the film by ±10° dramatically reduces the reflection intensity shown on the 2D GISAXS patterns (Supporting Information, Figure S5), which indicates the uniform orientation of the blades on the mica surface. However, owing to the cambered shape and the different domain of DNA packing in different blades (inset model of Figure $1c_3$), the diffraction patterns show domain structures with variations in the growth directions. The fan-shape integrations of the 2D patterns with a certain width also illustrate the rotation angle-dependent result (Figure 2A). The reflections with a *d*-spacing ratio of about $\sqrt{2}$ can be indexed to 10 and 11 reflections with the unit cell parameter $a \approx 2.5$ nm, which indicates the highly ordered 2D square mesostructure. The structure was later confirmed by the transmission electron microscopy (TEM) observations. The diffuse reflectance circular dichroism (DRCD) spectra of the dense (Figure 2B b) and sparse OCDSF (Figure 2B c) confirm the chiral property of the oriented film. The spectra show negative peaks at 295 nm and strong positive peaks at approximately 350 nm, whereas the ADSF does not show an obviously strong CD signal (Figure 2B a). For the chiral DNA–silica films, two kinds of OAs, the absorption-based OA within the absorption band of DNA molecular aggregation and the scattering-based

OA resulted from the chiral superstructure, would be observed.[10] The negative signals at approximate of 295 nm correspond to a resonance phenomenon from the absorption of the chromophores of the left-handed DNA long-range packing.[10,18] The positive signals at 350 nm result from the superposition of scattering OA of the left-handed twisted petals and right-handed distortion of the stacking, while the right-handed structure may show a dominating effect.[10] The scattering-based OA was further confirmed by the intensity decrease when immerse the film into optically isotropic solution (water and ethanol; Supporting Information, Figure S6A), owing to the refractive index n matching effect ($n_{SiO_2} = 1.46$, $n_{DNA} \approx 1.65$ (depending on the physical state),[19] $n_{H_2O} = 1.33$, $n_{EtOH} = 1.37$; a detailed representation is shown in the Supporting Information).[4a,20] However, as mica is a birefringent material, weak signals can be observed from the pure substrates (Supporting Information, Figure S7), indicating that the DRCD signal of the ADSF would not be zero.

The relationship between the chiral properties of the blades and the structure of the DNA self-assemblies in the oriented films was confirmed by TEM (Figure 3a–f). The sample was prepared by carefully scraping the blade of the sparse film from the substrate. As shown in Figure 3b, when the structure is aligned to an incident electron beam, a typical contrast of the 2D packing DNA–silica complex with plane group *p4mm* can be observed, which corresponds with the GISAXS results. As the whole blade exhibits hierarchical chiral structure with both left-handed and right-handed chirality, five domains of the blade were aligned to the electron beam by tilting the sample, and a twisted arrangement can be revealed. The parts c can be aligned by tilting the sample by 24.2° (Figure 3c, where the tilting axis is shown in the inset frame). The decomposed rotation angle along the *b* to *c* axis (red arrow in Figure 3a) is calculated to be anticlockwise 9.9°, indicating a left-handed twisting along the long axis of the petals. Similarly, part e is aligned by tilting by 20.4° (Figure 3e). The decomposed angle along the d to e axis (blue arrow in Figure 3a) is anticlockwise 17.3°, confirming the left-handed property of the petals. From part d to b then to f (green arrow, Figure 3a), the clockwise rotation angle is calculated to be 1.4°, revealing the slightly right-handed distortion along the horizontal long axis of the whole blade. Thus, the mesostructure of the blade agrees with the model shown in Figure 3, which indicates the left-handed DNA packing in the composing petals and right-handed stacking of the twisted petals to form the final individual chiral blades. Moreover, considering the vertical epitaxial growth direction of the blades and that the 2D square DNA–silica channels are perpendicular to the blades, it can be concluded that the long axes of the DNA molecules in each blade run largely parallel to the surface of the mica sheet and perpendicular to the direction of the blades.

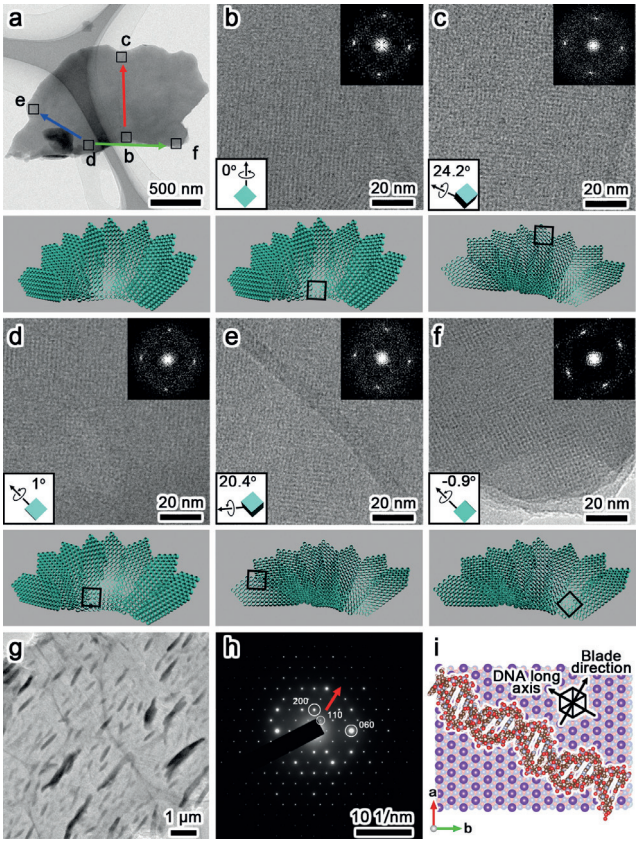

Figure 3. a) Low magnification TEM image of a chiral blade scraped from the sparse film. b)–f) HRTEM images and the Fourier diffractograms corresponding to the framed parts in (a); The tilting angle of different parts are shown in the inset frame. g) TEM images of a piece of the sparse OCDSF film showing the growth orientation of the film, h) Electron diffraction of the mica substrate supporting the film, and i) The corresponding model of DNA direction on the substrate.

To interpret the relationship between the orientation of the blade and the crystal structure of the mica, a piece of sparse film along with the thin mica substrate was peeled off from the substrate and observed by TEM (Figure 3g–i). Low-magnification TEM image shows the uniform direction of the blades on the mica surface (Figure 3g). The electron diffraction pattern of the whole area indicates that the underlay mica is a single crystal grown along the *ab*-plane. The blades are uniformly aligned along the [110] direction of the mica crystal (Figure 3h). As the DNA molecules are packed perpendicular to the blade, the long axes of DNA molecules follow the 2D hexagonal pattern of the Mg^{2+} ions on the mica surface. Considering that the B-form DNA is a right-handed double helix composed of 10 base pairs per pitch with the same base-pair separation of 3.4 Å, this anisotropic oriented absorption of DNA molecules is supposed to be determined by the nearest phosphate groups approaching the mica surface. As two adjacent phosphate groups on the same strand is about 120° to the DNA long axis, the positions of the nearest phosphate groups at the phosphate backbones of minor grooves and major grooves fit with the anchored Mg^{2+} in the mica lattice along the diagonal axis of the hexagonal lattice, providing efficient electrostatic interaction to anchor and align the DNA molecules along the 2D hexagonal lattice (see the Supporting Information, Figure S8 for details). From the point of view of the 2D crystal surface, the 2D hexagonal structure has three equal diagonal axes, which provides three possible directions for DNA alignment. This explains the infrequently observed direction rotation of nearly 120° of the

different adjacent domains (Supporting Information, Figure S9), which would occupy the three equivalent axes of the hexagonal pattern on the mica surface.

The considerable morphological differences between the films synthesized with or without Mg^{2+} prompted us to consider the effects of the Mg^{2+} ions on orientation. It has been reported that the absorption of DNA on mica was greatly affected by the bridging effect of metal counterions.[21] Atomic force microscopy (AFM) was used to prove the existence of the guiding effect of the DNA-Mg^{2+} monolayer on the subsequent silicification (Supporting Information, Figure S10). Strips of DNA molecular aggregations on mica substrates adopt a transformation from random to uniform orientation with the increasing of Mg^{2+} ions. The guiding effect of the molecular layer is further supported by the SEM images of the films produced with different concentrations of Mg^{2+} ions (Supporting Information, Figure S11). Increasing the Mg^{2+} content leads to an improved alignment of the film, suggesting the key influence of Mg^{2+} ions.

According to the results described above, the formation mechanism of the OCDSF was hypothesized based on the "mica-Mg^{2+}-DNA–silica quartet templating" route (Scheme 1). It is known that cleaved sheets of muscovite mica have about 2.1×10^{14} negative charges per cm^2, which are balanced by surface K^+ ions.[22] The Mg^{2+} ions can anchor on the substrate surface by ionic exchange with the K^+ ions and then reverse the negative charge into a positive charge, motivating interaction between the mica surface and the negatively charged DNA.[21a,23] Therefore, first, the Mg^{2+} ions replicate the original hexagonally arrangement of K^+ ions, then affects the absorption positions of DNA molecules, whose long axis is along the diagonal axis of the hexagon. The result is a DNA molecular aggregation layer (Scheme 1 a), which is similar to the assembled orientation of surfactant molecules that is guided by the crystal orientation of mica.[12b,c] The electron-screen effect of the Mg^{2+} ions on negatively charged DNA deposited the DNA-Mg^{2+} layers on the surface. Meanwhile, the stronger repulsive force between charged DNA molecules resulted in their parallel arrangement. Second, the molecular layer then acts as an adherent landing site that accretes and organizes the DNA aggregates packed by the polycations of the TMAPS condensation networks with a preferential orientation (Scheme 1 b). The positively charged TMPAS electrostatic interacts with the negatively charged phosphate of DNA molecules, acts both as condensation agent of DNA and the co-structure directing agent between templates and silica source TEOS. Here, the excess Mg^{2+} ions in solution break the charge equilibrium of TMAPS and DNA and act on the dislocated DNA array to induce the chiral packing, which induces the chiral structure of the OCDSF.[10,24] Moreover, the silane group of TMAPS near the substrate dehydration reacts with the extra native hydroxy groups of mica, which immobilize the aggregates. Third, the co-condensation of TMAPS and TEOS around the DNA template forms a rigid silica channel wall, leading to the epitaxial oriented growth of a long-range 3D architecture, as illustrated in Scheme 1 c. However, in the absence of Mg^{2+} ions, the anchoring of TMAPS on the mica surface is random, which cannot contribute to the uniformly aligned growth of individual DNA–silica plates. As a result, no preferred orientation would result. According to this mechanism, other divalent alkaline metal ions, Ba^{2+} and Sr^{2+}, also succeeded in orienting the chiral films (Supporting Information, Figure S12).

In conclusion, we have successfully oriented and arranged mesostructured helical DNA–silica assemblies into large-scale chiral films with long-range ordering utilizing the "quartet templating" pathway. The ordered transferring from a highly organized natural crystal to epitaxial patterns provides an efficient route to arrange the biomolecules in

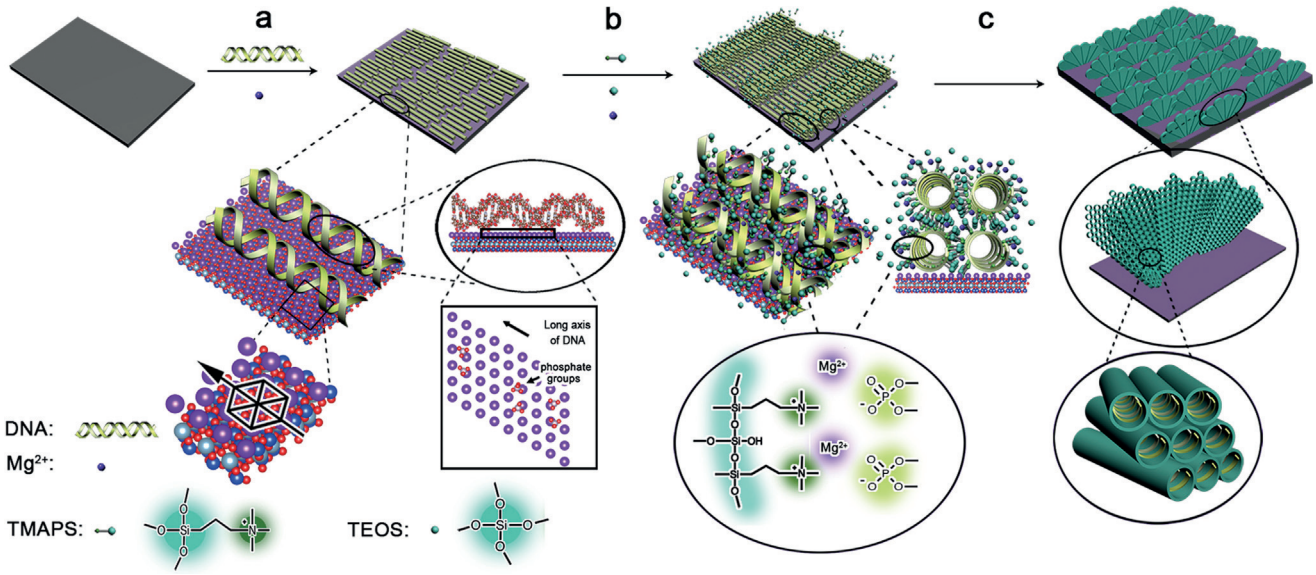

Scheme 1. Representation of the formation of the OCDSF. a) The formation of oriented DNA molecular layer on the surface of Mg^{2+} anchored mica sheets by the quartet templating mechanism. b) Sequential DNA chiral packing aggregates induced by TMAPS and Mg^{2+}. c) Growth of mesostructured chiral DNA–silica assembles with long-range horizontal parallel arrangement by silica mineralization.

chiral mesostructures and further develops the fabrication of nanostructure molds. We expect that this simple and powerful route will establish an avenue for the production of ordered chiral organic–inorganic films. Furthermore, the method would permit wider fabrication of chiral devices, such as broadband polarization devices, liquid crystal displays, or negative reflection materials, and would facilitate the ability to scale up to 3D organizations combining template-assisted self-assembly.

Acknowledgements

This work was supported by the National Natural Science Foundation of China (21471099, 21201120), Youth Natural Science Foundation of Shanghai (12ZR1445100), "Chenguang" program of the Shanghai Educational Development Foundation (12CG10). We thank the Instrumental Analysis Centre of Shanghai Jiao Tong University for their collaboration on the DRCD measurements.

Keywords: chiral films · controllable orientation · DNA self-assembly · mesoporous films · mica

How to cite: *Angew. Chem. Int. Ed.* **2016**, *55*, 2037–2041
Angew. Chem. **2016**, *128*, 2077–2081

[1] a) R. J. Kershner, L. D. Bozano, C. M. Micheel, A. M. Hung, A. R. Fornof, J. N. Cha, C. T. Rettner, M. Bersani, J. Frommer, P. W. K. Rothemund, et al., *Nat. Nanotechnol.* **2009**, *4*, 557–561; b) A. M. Hung, C. M. Micheel, L. D. Bozano, L. W. Osterbur, G. M. Wallraff, J. N. Cha, *Nat. Nanotechnol.* **2010**, *5*, 121–126; c) A. K. G. Tavakkoli, K. W. Gotrik, A. F. Hannon, A. Alexander-Katz, C. A. Ross, K. K. Berggren, *Science* **2012**, *336*, 1294–1298; d) R. K. Joshi, J. J. Schneider, *Chem. Soc. Rev.* **2012**, *41*, 5285–5312.

[2] Y. Wang, J. Xu, Y. Wang, H. Chen, *Chem. Soc. Rev.* **2013**, *42*, 2930–2962.

[3] a) J. K. Gansel, M. Wegener, S. Burger, S. Linden, *Opt. Express* **2010**, *18*, 1059–1069; b) J. K. Gansel, M. Thiel, M. S. Rill, M. Decker, K. Bade, V. Saile, G. von Freymann, S. Linden, M. Wegener, *Science* **2009**, *325*, 1513–1515.

[4] a) K. Robbie, D. J. Broer, M. J. Brett, *Nature* **1999**, *399*, 764–766; b) A. C. van Popta, J. C. Sit, M. J. Brett, *Appl. Opt.* **2004**, *43*, 3632–3639.

[5] I. Hodgkinson, *Adv. Mater.* **2001**, *13*, 889–897.

[6] a) O. Crespo-Biel, B. J. Ravoo, D. N. Reinhoudt, J. Huskens, *J. Mater. Chem.* **2006**, *16*, 3997–4021; b) Y. Yin, Y. Lu, B. Gates, Y. Xia, *J. Am. Chem. Soc.* **2001**, *123*, 8718–8729.

[7] H. Liang, T. E. Angelini, J. Ho, P. V. Braun, G. C. L. Wong, *J. Am. Chem. Soc.* **2003**, *125*, 11786–11787.

[8] a) K. M. M. Carneiro, F. A. Aldaye, H. F. Sleiman, *J. Am. Chem. Soc.* **2010**, *132*, 679–685; b) F. A. Aldaye, A. L. Palmer, H. F. Sleiman, *Science* **2008**, *321*, 1795–1799.

[9] B. Liu, Y. Yao, S. Che, *Angew. Chem. Int. Ed.* **2013**, *52*, 14186–14190; *Angew. Chem.* **2013**, *125*, 14436–14440.

[10] B. Liu, L. Han, Y. Duan, Y. Cao, J. Feng, Y. Yao, S. Che, *Sci. Rep.* **2014**, *4*, 4866.

[11] a) R. Fan, S. Huh, R. Yan, J. Arnold, P. Yang, *Nat. Mater.* **2008**, *7*, 303–307; b) N. Mojarad, J. Gobrecht, Y. Ekinci, *Microelectron. Eng.* **2015**, *143*, 55–63; c) B. J. Lin, *Microelectron. Eng.* **2015**, *143*, 91–101.

[12] a) B. Jérôme, Y. Shen, *Phys. Rev. E* **1993**, *48*, 4556–4574; b) H. Yang, A. Kuperman, N. Coombs, S. Mamiche-Afara, G. A. Ozin, *Nature* **1996**, *379*, 703–705; c) T. Suzuki, Y. Kanno, Y. Morioka, K. Kuroda, *Chem. Commun.* **2008**, 3284–3286; d) H. N. Patrick, G. G. Warr, S. Manne, I. A. Aksay, *Langmuir* **1999**, *15*, 1685–1692.

[13] a) J. Kim, C. Bayram, H. Park, C.-W. Cheng, C. Dimitrakopoulos, J. A. Ott, K. B. Reuter, S. W. Bedell, D. K. Sadana, *Nat. Commun.* **2014**, *5*, 4836; b) W. C. Lee, *Nat. Nanotechnol.* **2015**, *10*, 423–428.

[14] H. Miyata, K. Kuroda, *J. Am. Chem. Soc.* **1999**, *121*, 7618–7624.

[15] a) D. Pastré, O. Piétrement, S. P. Fusil, F. Landousy, J. Jeusset, M.-O. David, L. C. Hamon, E. Le Cam, A. Zozime, *Biophys. J.* **2003**, *85*, 2507–2518; b) M. F. Brigatti, A. Mottana, D. Malferrari, G. Cibin, *Am. Mineral.* **2007**, *92*, 1395–1400.

[16] S. Che, A. E. Garcia-Bennett, T. Yokoi, K. Sakamoto, H. Kunieda, O. Terasaki, T. Tatsumi, *Nat. Mater.* **2003**, *2*, 801–805.

[17] B. Liu, L. Han, S. Che, *Angew. Chem. Int. Ed.* **2012**, *51*, 923–927; *Angew. Chem.* **2012**, *124*, 947–951.

[18] F. Livolant, M. F. Maestre, *Biochemistry* **1988**, *27*, 3056–3068.

[19] T. Inagaki, *J. Chem. Phys.* **1974**, *61*, 4246–4250.

[20] K. E. Shopsowitz, H. Qi, W. Y. Hamad, M. J. MacLachlan, *Nature* **2010**, *468*, 422–425.

[21] a) M. Bezanilla, S. Manne, D. E. Laney, Y. L. Lyubchenko, H. G. Hansma, *Langmuir* **1995**, *11*, 655–659; b) H. G. Hansma, D. E. Laney, *Biophys. J.* **1996**, *70*, 1933–1939; c) Y. Song, Z. Li, Z. Liu, G. Wei, L. Wang, L. Sun, C. Guo, Y. Sun, T. Yang, *J. Phys. Chem. B* **2006**, *110*, 10792–10798.

[22] R. M. Pashley, J. N. Israelachvili, *J. Colloid Interface Sci.* **1984**, *97*, 446–455.

[23] X. Gong, A. Kozbial, L. Li, *Chem. Sci.* **2015**, *6*, 3478–3482.

[24] B. Liu, L. Han, S. Che, *J. Mater. Chem. B* **2013**, *1*, 2843–2850.

Received: September 28, 2015
Revised: November 28, 2015
Published online: January 6, 2016

